

Plasma Luminescence from Femtosecond Filaments in Air: Evidence for Impact Excitation with Circularly Polarized Light Pulses

Sergey Mitryukovskiy, Yi Liu, Pengji Ding, Aurélien Houard, Arnaud Couairon, André Mysyrowicz

► **To cite this version:**

Sergey Mitryukovskiy, Yi Liu, Pengji Ding, Aurélien Houard, Arnaud Couairon, et al.. Plasma Luminescence from Femtosecond Filaments in Air: Evidence for Impact Excitation with Circularly Polarized Light Pulses. *Physical Review Letters*, American Physical Society, 2015, 114, pp.63003. 10.1103/PhysRevLett.114.063003 . hal-01118358

HAL Id: hal-01118358

<https://hal-ensta-paris.archives-ouvertes.fr//hal-01118358>

Submitted on 18 Feb 2015

HAL is a multi-disciplinary open access archive for the deposit and dissemination of scientific research documents, whether they are published or not. The documents may come from teaching and research institutions in France or abroad, or from public or private research centers.

L'archive ouverte pluridisciplinaire **HAL**, est destinée au dépôt et à la diffusion de documents scientifiques de niveau recherche, publiés ou non, émanant des établissements d'enseignement et de recherche français ou étrangers, des laboratoires publics ou privés.

Plasma luminescence from femtosecond filaments in air: evidence for impact excitation with circularly polarized light pulses

Sergey Mitryukovskiy¹, Yi Liu^{1,*}, Pengji Ding¹, Aurélien Houard¹, Arnaud Couairon², and André Mysyrowicz^{1,§}

¹ Laboratoire d'Optique Appliquée, ENSTA/CNRS/Ecole Polytechnique, 828, Boulevard des Maréchaux, Palaiseau, F-91762, France

² Centre de Physique Théorique, Ecole Polytechnique, CNRS, Palaiseau, F-91128, France

* yi.liu@ensta-paristech.fr; § andre.mysyrowicz@ensta-paristech.fr

Abstract

Filaments produced in air by intense femtosecond laser pulses emit UV luminescence from excited N_2 and N_2^+ molecules. We report on a strong dependence at high intensities ($I \geq 1.4 \times 10^{14} \text{ W/cm}^2$) of this luminescence with the polarization state of the incident laser pulses. We attribute this effect to the onset of new impact excitation channels from energetic electrons produced with circularly polarized laser pulses above a threshold laser intensity.

PACS numbers: 33.50. Dq, 34.80. GS, 33.80. Rv

Intense femtosecond laser pulses launched in transparent media experience filamentary propagation, a generic phenomenon in solid, liquids, and gases [1, 2]. A distinctive signature of filamentation in air is the formation of a long, bright channel of under dense plasma in the wake of the propagating laser pulses. The length over which the plasma column is formed can vary between a few millimeters to hundreds of meters, depending on laser characteristics, although its length is limited to a few meters at any instant, because of the fast plasma recombination [1, 2]. Much interest has been devoted to the study of the luminescence of this plasma in air. As shown first by the group at Laval University, it differs from that obtained with laser pulses of longer duration [3]. Instead of Nitrogen and Oxygen atomic lines superimposed on a broad continuum, it consists of discrete lines due to excited nitrogen molecules. These lines correspond to transitions between excited triplet states $C^3\Pi_u^+$ and $B^3\Pi_g^+$ of neutral nitrogen molecules (2^{nd} positive system of N_2) and between second excited state $B^2\Sigma_u^+$ and ground state $X^2\Sigma_g^+$ of nitrogen molecular ions (1^{st} negative system of N_2^+) [3, 4]. A detailed understanding of the process leading to this filament luminescence is important for several reasons. Filament luminescence has been used as a tool to characterize the length and width of the plasma column and to extract the electron temperature and laser intensity inside filaments [5-8]. Due to its dependence on an external electric field, it has found application in the remote measurement of DC electric field or intense Terahertz radiation [9, 10]. A good understanding of its excitation process is also central to an interpretation of the recently discovered laser action from either neutral or ionized nitrogen molecules inside filament plasmas [11-17].

In this letter, we measure and discuss the dependence of the luminescence from both N_2 and N_2^+ molecules on polarization of the incident femtosecond laser pulse. It reveals new non radiative routes to populate excited neutral and ionic molecular levels through electron collisions. A minimum electron kinetic energy is necessary in order to achieve impact excitation of neutral or ionized molecules. In the range of laser intensities of this study, numerical simulations predict that this threshold kinetic energy is only obtained with circular polarization, in good agreement with our experimental observations.

In the experiment, femtosecond laser pulses with pulse energy up to 10 mJ (45 fs, 800 nm) from a commercial laser system (Thales Laser, Alpha 100) were focused by an $f = 1000$ mm convex lens in ambient air. A quarter-wave plate ($\lambda/4$) was installed before the focal lens to change the laser polarization from linear to circular. Plasma channels with length varying from a few millimeters to several centimeters were created, depending on the incident pulse energy. In order to detect the spontaneous luminescence, a lens of focal distance $f = 25$ mm was employed to collimate the luminescence emitted in the direction orthogonal to the laser propagation axis and a second lens with $f = 100$ mm was used to focus the collected emission onto the entrance slit of a monochromator (Jobin-Yvon H-20 UV). The two lenses used were made of fused silica. The luminescence signal from the monochromator was measured by a photomultiplier tube (Hamamatsu, model: H10722). In order to resolve longitudinally the luminescence signal along

the filament axis, a rectangular diaphragm (1 mm × 6 mm) was placed 1 mm away from the filament axis. More details about the detection method can be found in ref [17].

We first measured the luminescence spectrum for linearly and circularly polarized laser pulses at two representative incident laser pulse energies E_{in} . Detection was performed at the middle position of the plasma in each case. Figure 1 shows the results for $E_{in} = 250 \mu\text{J}$, just below the threshold for filamentation (Fig. 1(a)) and at 8.3 mJ, where the peak power is 30 times higher than the critical power for filamentation (Fig. 1(b)). The corresponding peak laser intensities were determined by measuring the laser flux and pulse duration transmitted through a circular diaphragms of 80 μm diameter placed in the middle of the plasma string. It yields $I = 3 \times 10^{13} \text{ W/cm}^2$ in case (a) and a value $I \geq 1.4 \times 10^{14} \text{ W/cm}^2$ for incident pulse energies above 1 mJ, when filaments are formed [17]. No significant difference of laser intensity was observed for linear and circular laser polarization. The luminescence lines visible in Figure 1 belong to two categories, as already mentioned: transitions between excited triplet states of the neutral nitrogen molecules or transitions between different ionic states N_2^+ of the nitrogen molecule [3]. Their precise identification in terms of rotational levels is given Fig. 1. As can be seen, upon increase of laser intensity, there is a reversal in the relative intensity of luminescence between linear and circular pump laser polarization. At lower intensities, linearly polarized pump light is more efficient. At higher laser intensity, a circularly polarized pump becomes more effective.

The same trend is better observed in the dependence of the 337 nm (representative of luminescence from neutral molecules) and 391 nm signals (due to molecular ion emission) as a function of pump laser ellipticity. The ellipticity ε of the laser can be changed continuously from linear ($\varepsilon = 0$) to elliptical ($0 < \varepsilon < 1$), and circular ($\varepsilon = 1$) by rotating the quarter-wave plate. In Fig. 2, results are presented for 4 different pulse energies as a function of rotation angle of the $\lambda/4$ waveplate. The angles $\varphi = 90^\circ \times m$ correspond to linearly polarized laser, with $m = 0, 1, 2, 3$. The angles $\varphi = 45^\circ + 90^\circ \times m$ correspond to circular laser polarization. All measurements were performed around the center of the plasma. With a laser pulse energy of 250 μJ , the dominance of linear laser polarization over elliptical and circular is observed for both 337 nm and 391 nm emission lines (Fig. 2(a) and 2(a')). With a pulse energy of 600 μJ , the intensity of the triplet luminescence line at 337 nm becomes independent of the pump polarization (Fig. 2(b)). Upon a further increase of the pump pulse energy, the signal at 337 nm becomes more intense with a circularly polarized pump (Fig. 2(c) and 2(d)). Concerning the emission of N_2^+ at 391 nm, its relative intensity increases with circularly polarized laser pulses (see Fig. 2(b') and 2(c')), until almost no dependence on ellipticity is observed for pulses of 10 mJ (Fig. 2(d')).

In Fig. 3, we present the evolution of luminescence lines at 337 nm and 391 nm along the filament axis z for both linear and circular laser polarization, again for three different incident laser pulse energies. Below the threshold for filamentation (Fig. 3(a) and (a')), the length of the plasma corresponds to the Rayleigh distance calculated by assuming a linear laser pulse propagation. As expected for such a case, the plasma luminescence peaks at the geometric focus. Both lines are more intense along the ~ 25 mm plasma string with linearly polarized pump. At higher laser energies ($E_{in} = 1.1$ mJ), the plasma string moves towards the laser, a signature of filamentation (Fig. 3(b) and 3(b')). The luminescence obtained with circularly polarized light increases and becomes equal or even predominant at still higher energies ($E_{in} = 10$ mJ), (Fig. 3(c) and 3(c')). We verified that other emission lines at 357 nm and 428 nm exhibit a similar behavior.

How should we understand the dependence of the luminescence with pump laser polarization? Populating excited ionic state $N_2^+(B^2\Sigma_u^+)$ during filamentation in air is generally accepted as being due to direct high-field photon-ionization of inner-valence electrons of the nitrogen molecules [18, 19]. Linear laser polarization is known to be more efficient [18, 19]. Direct high-field photonic excitation of the triplet state $N_2(C^3\Pi_u^+)$ is a spin forbidden process and therefore unlikely. Two indirect excitation processes have been proposed. A first scheme consists in a dissociative recombination through the processes: $N_2^+ + N_2 + N_2 \rightarrow N_4^+ + N_2$ followed by $N_4^+ + e \rightarrow N_2(C^3\Pi_u^+) + N_2$ [20]. Another more recent scenario proposes that collision-assisted intersystem crossing from excited singlet states is the dominant path to produce the triplet state, while the dissociative recombination would be a minor contributor [21]. In any case, both processes should generate a larger signal with a linearly polarized pump. In the case of dissociative recombination, the final density of $N_2(C^3\Pi_u^+)$ molecules depends on the density of N_2^+ , which is more effectively produced by linearly polarized laser in the laser regime of 10^{13}

$\text{W}/\text{cm}^2 - 10^{15} \text{W}/\text{cm}^2$ [18, 19]. With the intersystem crossing mechanism, one expects a similar dependence on laser polarization, because the transition from the fundamental singlet state of N_2 to an intermediate singlet state is more effective with linearly polarized laser pulses. So the question is why circularly polarized laser pulses become more efficient at higher laser intensity?

An important difference between linear and circular laser polarization in gas plasma generation is the kinetic energy of free electrons remaining after the passage of the intense laser field [22, 23]. With linearly polarized laser pulses, free electrons are left with low kinetic energy because they experience alternative acceleration and deceleration by the laser field during each optical cycle of the pulse. By contrast, with a circularly polarized laser, electrons are always accelerated away from the molecular ion. As discussed below, free electrons acquire an average energy of $\sim 2U_p$ at the end of the laser pulse, where $U_p = e^2/c\epsilon_0 m_e \times I/2\omega_0^2$ is the ponderomotive energy of the electron in the laser field with ϵ_0 , m_e , I , ω_0 being the vacuum permittivity, the mass of the electron, the intensity and frequency of the laser field. Therefore, a large number of electrons with a kinetic energy around $2U_p \geq 16.7 \text{ eV}$ are produced inside a filament.

The distribution of transverse electron kinetic energies can be predicted by semi-analytical laws: integration of Newton's equations for electron motion leads to a transverse momentum $\vec{p}(t) = -e(\vec{A}(t) - \vec{A}_0)$, where $\vec{A}(t)$ denotes the vector potential at instant t and \vec{A}_0 denotes its counterpart when the electron is liberated, at rest. After the passage of the pulse, $\vec{A}(t)$ vanishes. The transverse momentum becomes $p(\infty) = -eA_0$, and the transverse kinetic energy reads $E_{kin}(t_0) = e^2 A_0^2/2m$, where t_0 indicates that the electron was liberated at instant t_0 within the pulse. We can infer the vector potential by integration of $\vec{E} = -\partial\vec{A}/\partial t$ by using an analytical form for the electric field with a cosine envelope

$$E = \begin{cases} E_0 \cos\left(\frac{\pi}{Tc}\right) \left[\cos\left(\frac{\omega_0 t}{c} + \theta\right) \vec{u}_x + \varepsilon \sin\left(\frac{\omega_0 t}{c} + \theta\right) \vec{u}_y \right] & \text{for } -T/2 < t < T/2 \\ 0 & \text{For } t < -T/2 \text{ and } t > T/2 \end{cases} \quad (1)$$

where θ denotes an arbitrary carrier envelope phase. The kinetic energy of an electron, born at time t_0 when the electric field phase $\phi \equiv (\omega_0/c)t = \phi_0$, after acceleration by the pulse can therefore found to be

$$E_{kin} = 2U_p \cos^2 u \phi_0 [1 - (1 - e^2) \cos^2(\phi_0 + \theta)] \quad (2)$$

potential. Therefore, all electrons generated between t_0 and $t_0 + \Delta t$, with probability $(\partial n_e/\partial t)_{t_0} \times (\Delta t/n_{e,\infty})$, where $n_e(t)$ denotes the electron density calculated from the rate equations and $n_{e,\infty}$ denotes the total electron density generated by the pulse, will have a kinetic energy between $E_{kin}(t_0)$ and $E_{kin}(t_0 + \Delta t)$. We retrieve that the maximum kinetic energy of the electrons is $2U_p$ for a circularly polarized pulse ($\varepsilon = 1$) when it is born at the peak of the field envelope ($t = 0$). A parametric representation of the distribution of kinetic energies is presented as a continuous curve in Fig. 4. In the case of linear laser polarization most electrons are left with energy below 1 eV, as shown in Fig. 4 (a). By contrast, an almost monoenergetic distribution around 16.7 eV is achieved for circular laser polarization (Fig. 4(b)) [24]. We also calculated the electron energy distribution after the passage of the laser pulses by numerical simulations. In the simulations, we assume that electrons are generated by optical field ionization of oxygen and nitrogen molecules, described by a set of coupled rate equations. At the intensity level considered, we also computed second ionization processes so as to accurately determine the fraction of oxygen and nitrogen ions which liberate a second electron and found them negligible. Liberated electrons are assumed at rest and are accelerated by the electromagnetic (Lorentz) force mainly in the polarization plane. The acceleration in the longitudinal (propagation) direction is negligible compared to the transverse acceleration. We calculated the classical motion of a set of electrons under the action of the Lorentz force and then performed statistics by weighting each electron by its probability to be liberated at a given instant during the pulse. The results of these numerical simulations are presented by the bars in Fig. (4) and agree very well with that of the semi-analytical analysis.

Electrons with high kinetic energy can populate excited states of N_2 and N_2^+ via a collision process. Process $\text{N}_2(X^1\Sigma_g^+) + e \rightarrow \text{N}_2(C^3\Pi_u^+) + e$ populating the triplet molecular state opens up if the electron energy exceeds a rather sharp threshold energy of $\sim 11 \text{ eV}$, with a cross section peaking at 14.5 eV with a value of 0.58 \AA^2 [25]. In a traditional nitrogen laser pumped by electric discharge, it is actually this inelastic collision that gives rise to population inversion between the $C^3\Pi_u^+$ and $B^3\Pi_g^+$ states [26]. In our case, the energetic electrons produced inside

the filament plasma with circularly polarized laser pulse lead to efficient population build-up in the $C^3\Pi_u^+$ state, and thus stronger luminescence at 337 nm, as observed in Fig. 2(d) and Fig. 3(c). They experience collisions with neutral air molecules at frequency $\nu_c \sim 10^{12}$ Hz for standard temperature and pressure conditions. In the presence of abundant energetic free electrons, electron collision excitation of the excited ionic state $B^2\Sigma_u^+$ is also possible through the process $N_2(X^1\Sigma_g^+) + e \rightarrow N_2^+(B^2\Sigma_u^+) + 2e$. The corresponding threshold electron energy is 18.75 eV with a maximum effective collision section of $\sim 0.01 \text{ \AA}^2$ at [25, 27, 28]. With circularly polarized laser pulses of intensity $I = 1.4 \times 10^{14} \text{ W/cm}^2$, energetic electrons just reach the required energy.

We have verified the interpretation of new collision-induced excitation routes by repeating at low air pressure the ellipticity measurements shown in Fig. 2. Low gas pressure effectively suppresses collisions and therefore is also expected to suppress the corresponding excitation routes. Result is shown in Fig. 5 for line at 337 nm at a gas pressure of 10 mbar and a laser pulse energy of 350 μJ . Since the propagation of the pulse is linear at such a low pressure, the intensity at the focus can be readily estimated from diffraction to be $1.45 \times 10^{14} \text{ W/cm}^2$, of same order of magnitude as in a filament at normal pressure. As can be seen, the response to ellipticity is the same as that observed at lower intensities (Fig. 2(a)) although the reason is different. At normal pressure, collisions are present, but the electron energy is insufficient to excite the molecules (Fig. 2(a)); at low pressure (Fig. 5), electrons have the required kinetic energy but collisions are suppressed. A similar result is obtained for line at 391nm when the laser pulse energy is varied between 250 and 500 μJ .

In conclusion, we have demonstrated that the luminescence emitted by neutral and singly ionized N_2 molecules inside femtosecond laser filaments in air depends strongly on the polarization state of the incident laser pulses. At lower laser pump energies, the predominance of the luminescence from both species with linearly polarized pump is simply explained by the higher optical field ionization rate that constitutes the prime excitation route. At higher laser intensity, new excitation routes become available, due to the presence of electrons with high kinetic energy left after the laser pulse. A collision-assisted mechanism populates the excited triplet state of N_2 and the excited ionic molecular state of nitrogen directly from the ground state of neutral molecules. These findings are important for the understanding of the stimulated radiation from filaments and may find applications in remote sensing of electric field and THz radiation. We believe that these findings are not just restricted to laser filamentation process and they should intervene in other laser-gas interaction phenomenon, such as laser-induced gas breakdown and its relevant applications.

References:

1. A. Couairon, A. Mysyrowicz, Phys. Rep. **441**, 47 (2007).
2. S. L. Chin, S. A. Hosseini, W. Liu, Q. Luo, F. Th  berge, N. Ak  zbek, A. Becker, V. P. Kandidov, O. G. Kosareva, and H. Schroeder, Can. J. Phys. **83**, 863 (2005).
3. A. Talebpour, S. Petit, S. L. Chin, Opt. Commun. **171**, 285 (1999).
4. F. Martin, R. Mawassi, F. Vidal, I. Gallimberti, D. Comtois, H. Pepin, J. C. Kieffer, H. P. Mercure, Appl. Spectrosc. **56**, 1444 (2002).
5. S. A. Hosseini, Q. Luo, B. Ferland, W. Liu, N. Ak  zbek, G. Roy, and S. L. Chin, Appl. Phys. B **77**, 697 (2003).
6. A. Filin, R. Compton, D. A. Romanov, and R. J. Levis, Phys. Rev. Lett. **102**, 155004 (2009).
7. L. Shi, W. Li, Y. Wang, X. Lu, L. Ding, and H. Zeng, Phys. Rev. Lett. **107**, 095004 (2011).
8. S. Xu, X. Sun, B. Zeng, W. Chu, J. Zhao, W. Liu, Y. Cheng, Z. Xu, and S. L. Chin, Opt. Express **20**, 299 (2012).
9. J. Liu, J. Dai, S. L. Chin, X.-C. Zhang, Nat. Photon. **4**, 627 (2010).
10. K. Sugiyama, T. Fujii, M. Miki, M. Yamaguchi, A. Zhidkov, E. Hotta, and K. Nemoto, Opt. Lett. **34**, 2964 (2009).
11. A. Dogariu, J. B. Michael, M. O. Scully, and R. B. Miles, Science **331**, 442 (2011).
12. J. Yao, B. Zeng, H. Xu, G. Li, W. Chu, J. Ni, H. Zhang, S. L. Chin, Y. Cheng, and Z. Xu, Phys. Rev. A **84**, 051802(R) (2011).
13. Q. Luo, W. Liu, and S. L. Chin, Appl. Phys. B **76**, 337 (2003).
14. D. Kartashov, S. Ali  sauskas, G. Andriukaitis, A. Pug  lys, M. Shneider, A. Zheltikov, S. L. Chin, and A. Baltu  ska, Phys. Rev. A **86**, 033831 (2012).

15. G. Point, Y. Liu, Y. Brelet, S. Mitryukovskiy, P. Ding, A. Houard, and A. Mysyrowicz, *Opt. Lett.* **39**, 1725 (2014).
16. Y. Liu, Y. Brelet, G. Point, A. Houard, and A. Mysyrowicz, *Opt. Express*, **21**, 22791 (2013).
17. S. Mitryukovskiy, Y. Liu, P. Ding, A. Houard and A. Mysyrowicz, *Opt. Express* **22**, 12750 (2014).
18. A. Talebpour, A. Bandrauk, and S. L. Chin, in: L. F. Dimauro, R. R. Freeman, K. C. Kulander (Eds.), *Multiphoton Processes*, AIP, New York, 508 (2000).
19. A. Becker, A. D. Bandrauk, and S. L. Chin, *Chem. Phys. Lett.* **343**, 345 (2001).
20. H. L. Xu, A. Azarm, J. Bernhardt, Y. Kamali, and S. L. Chin, *Chem. Phys.* **360**, 171 (2009).
21. B. R. Arnold, S. Roberson, and P. M. Pellegrino, *Chem. Phys.* **405**, 9 (2012).
22. P. H. Bucksbaum, M. Bashkansky, R. R. Freeman and T. J. McIlrath, and L. F. DiMauro, *Phys. Rev. Lett.* **56**, 2590 (1986).
23. P. Corkum, N. H. Burnett, and F. Brunel, *Phys. Rev. Lett.* **62**, 1259 (1989).
24. See our supplementary materials.
25. Y. Itikawa, *J. Phys. Chem. Ref. Data.* **35**, 31 (2006).
26. R. S. Kunabenchi, M. R. Gorbali, and M. I. Savadatt, *Prog. Quantum Electron.* **9**, 259 (1984).
27. D. H. Crandall, *et al*, *Phys. Rev. A* **9**, 2545 (1974).
28. O. Nagy, *Chem. Phys.* **286**, 109 (2003).

Figure captions:

Fig. 1. Luminescence spectrum of the air plasma filaments for linearly and circularly polarized laser pulses of 250 μJ (a) and 8.3 mJ (b). In (a), the signal obtained with circular laser polarization is multiplied by a factor of 2 for visibility. The measurements in (a) and (b) were performed at $z = -2$ mm and -45 mm respectively (see Fig. 3(a)). The vibration quantum numbers related to the second positive system of the N_2 and the first negative system of N_2^+ are denoted.

Fig. 2. Luminescence at 337 nm ((a)-(d)) and 391 nm ((a')-(d')) as a function of the rotation angle of the quarter-wave plate. The incident pulse energy was 250 μJ , 600 μJ , 2.7 mJ and 10 mJ for (a) and (a'), (b) and (b'), (c) and (c'), (d) and (d'), respectively. All the measurements were performed around the center of the filament. Angle 0° corresponds to linearly polarized light.

Fig. 3. Intensity of the 337 nm ((a)-(c)) and the 391 nm ((a')-(c')) luminescence signal measured along the filaments for linearly and circularly polarized laser pulses. The incident pulse energy was 250 μJ for (a) and (a'), 1.1 mJ for (b) and (b'), and 10 mJ for (c) and (c').

Fig. 4. Calculated electron energy distribution in the case of linearly (a) and circularly (b) polarized laser pulses. The laser intensity used in the calculation was 1.4×10^{14} W/cm^2 . The red lines represent analytic results and the bars numerical simulation.

Fig. 5. Luminescence at 337 nm as a function of the rotation angle of the quarter-wave plate for air pressure of 10 mbar. The incident pulse energy was 350 μJ and the calculated laser intensity is 1.45×10^{14} W/cm^2 .

Figure 1

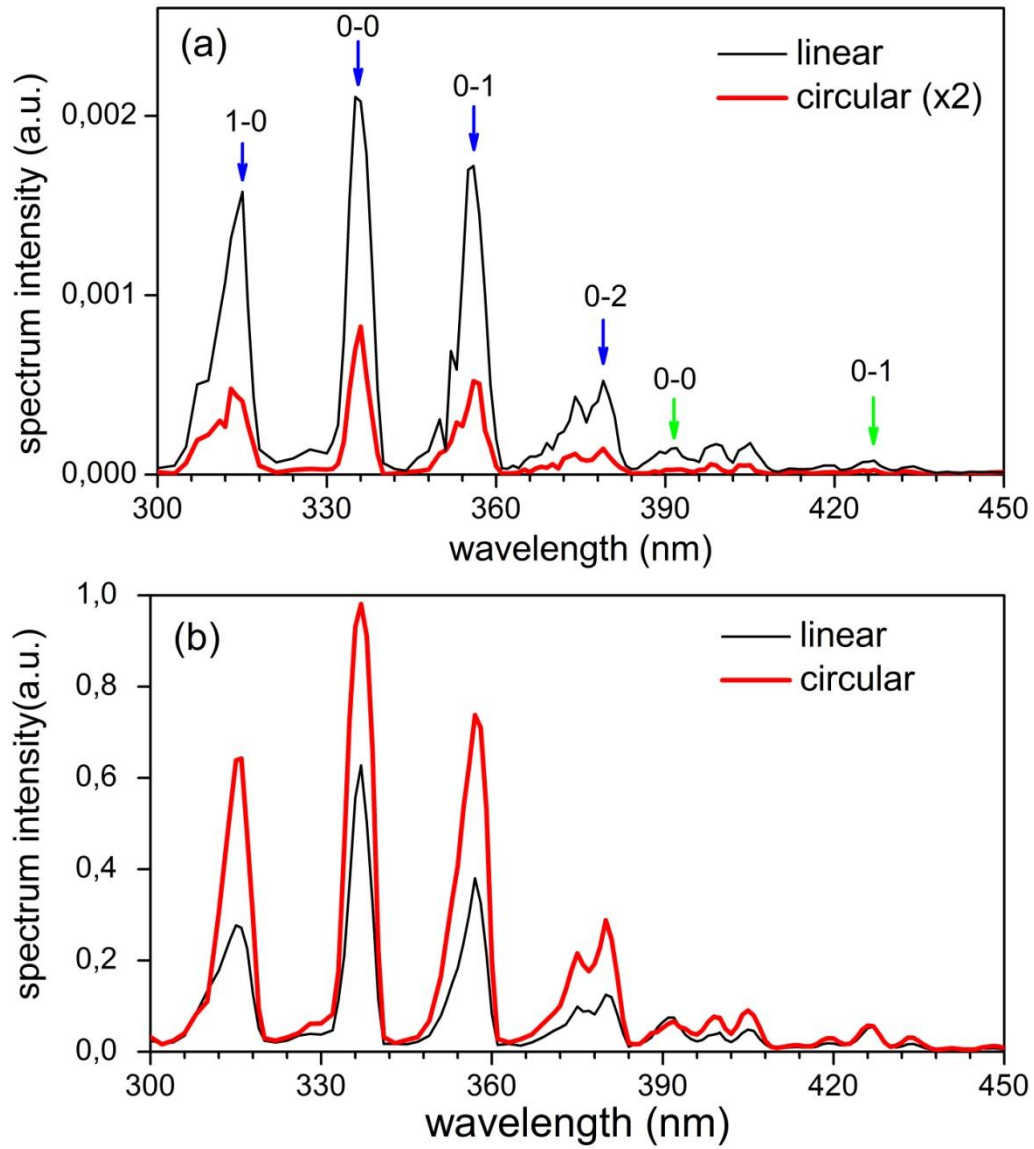


Figure 2

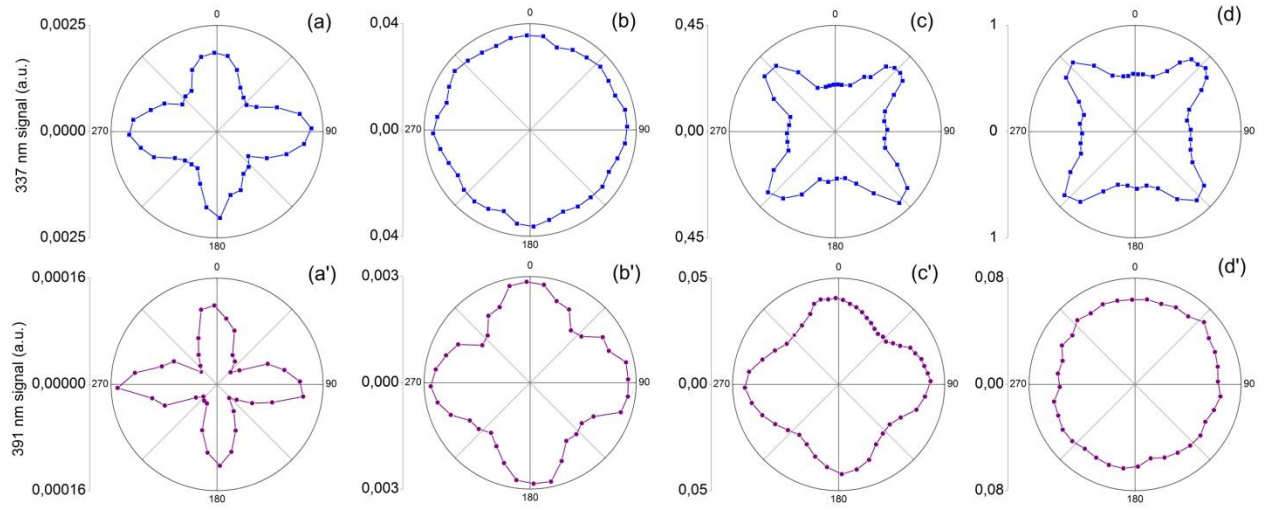


Figure 3

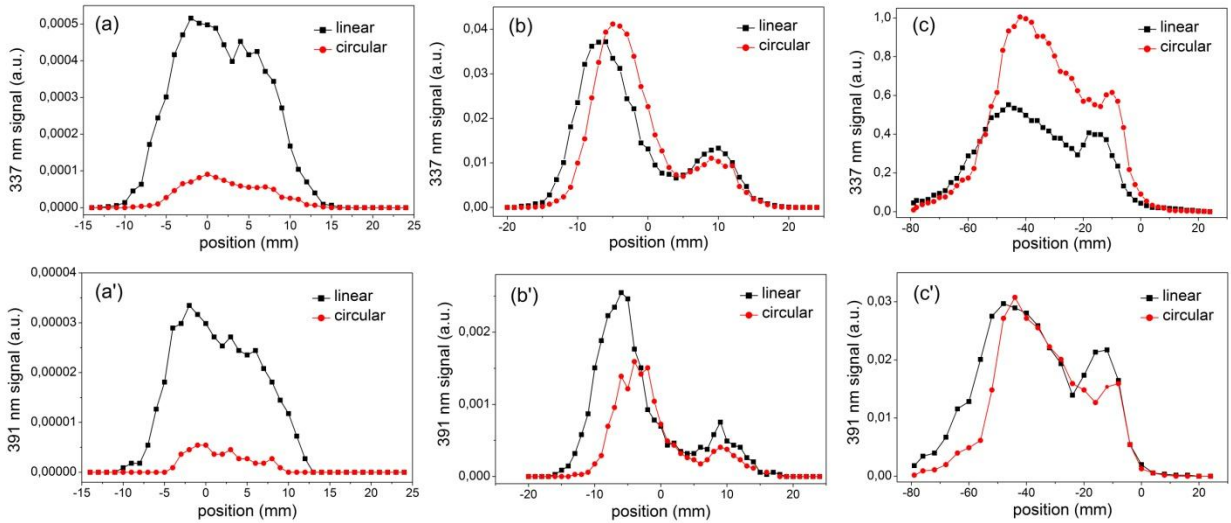


Figure 4

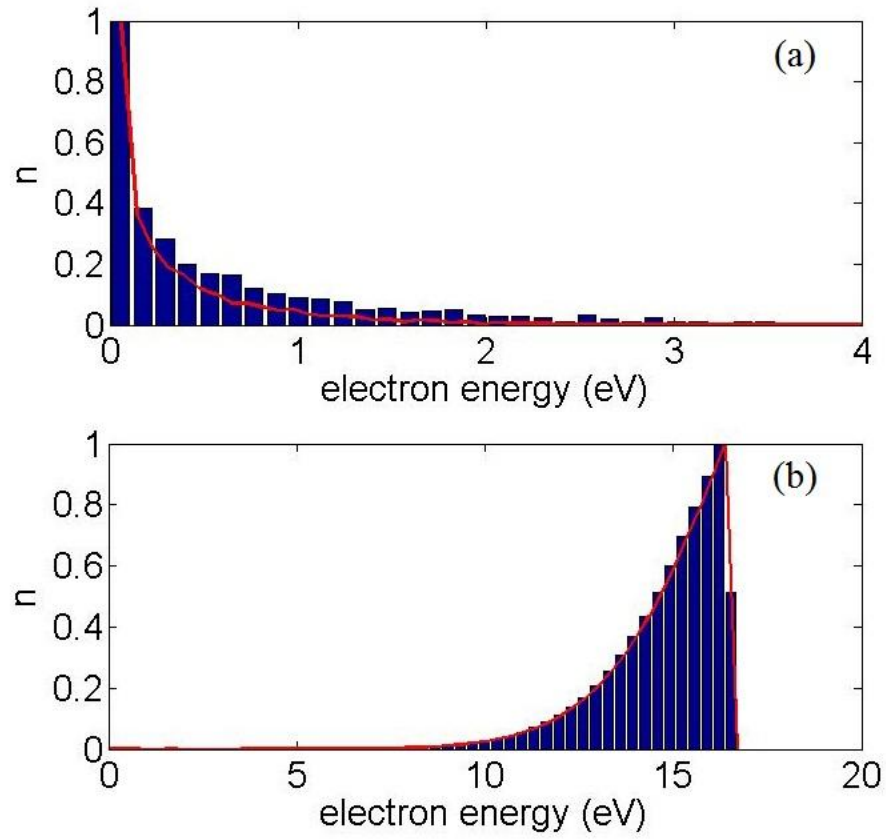


Figure 5

